Harmonic patterns embedding ictal EEG signals in focal epilepsy: a new insight into the epileptogenic zone

Lingli Hu,[1,2] Lingqi Ye,[1] Hongyi Ye,[1] Xiaochen Liu,[3] Kai Xiong,[4] Yuanming Zhang,[3] Zhe Zheng,[5] Hongjie Jiang,[5] Cong Chen,[1] Zhongjin Wang,[1] Jiping Zhou,[6] Yingcai Wu,[4] Kejie Huang,[3] Junming Zhu,[2,5] Zhong Chen,[7] Ding Meiping,[1] Dongping Yang,[8]* Shuang Wang[1,2]*

Abstract

The ictal EEG biomarkers of the epileptogenic zone (EZ) require more precise definition. The ictal initial fast activity is important in EZ localization, but EEG onset patterns are heterogeneous and the fast activity is absent in many patients. Here we defined a unique spectral structure of “harmonic pattern” (H pattern) on stereo-EEG (SEEG), characterized by multiple equidistant, high-density bands with varying frequency on time-frequency map. The H pattern was commonly observed among 57 (81.4%) out of 70 patients with focal onset pattern on SEEG. It manifests in seizures with various ictal onset patterns with or without fast activities, occurring at either early or late stages of seizures. The H pattern was found to be embedded only in two types of EEG segments: fast activity with a frequency > 25 Hz (FA-H pattern) during early stage of seizure (mean 13.3 seconds after onset), and irregular polyspikes (> 5 Hz, PS-H pattern) observed during late stage (mean 23.3 seconds after onset). The H pattern is typically observed at a very proximate time point across the seizure onset zone (SOZ), the early propagation zone, and occasionally other areas, with the same

fundamental frequency, indicating an inter-regional synchronization. Notably, the SOZ exhibited the highest proportion of channels expressing H pattern, and also the highest band number of H pattern. At the patient level, the dominant H pattern was defined as those with high ranks in band numbers, specifically exceeding the third quartile (Q3). Resection of the region expressing dominant H pattern, but not SOZ, independently predicted seizure freedom after surgery. This suggests that the dominant H pattern serves as an ictal marker of EZ. The generation mechanism of the H pattern was then explored. Through nonlinear analysis, our data demonstrated that the H pattern was generated by specific nonlinear phenomena rather than being a result of frequency intermodulation or purely methodological artefact. The degree of nonlinearity was more pronounced in the dominant H pattern compared to non-dominant counterpart. We postulate that FA-H pattern may be sustained by a predominant and synchronized firing of GABAergic neurons, while excitatory neuron firing plays a more important role for PS-H pattern. As a distinctive and common ictal spectral feature, H pattern conveys unique information of ictal neural dynamics and provides new insights into the EZ. Our study additionally presents evidence supporting the existence of an elongated time-window for measuring EZ through quantitative EEG.

Author affiliations:

1 Department of Neurology and Epilepsy Center, Second Affiliated Hospital, School of Medicine, Zhejiang University, Hangzhou, China

2 Nanhu Brain-computer Interface Institute, Hangzhou, China

3 College of Information Science and Electronic Engineering, Zhejiang University,

Hangzhou, China

4 School of Computer Science and Technology, Zhejiang University, Hangzhou, China

5 Department of Neurosurgery, Second Affiliated Hospital, School of Medicine, Zhejiang University, Hangzhou, China

6 Department of Neurology, Wayne State University/Detroit Medical Center, Detroit, MI, USA

7 Key Laboratory of Neuropharmacology and Translational Medicine of Zhejiang Province, School of Pharmaceutical Sciences, Zhejiang Chinese Medical University, Hangzhou, China

8 Research Center for Augmented Intelligence, Research Institute of Artificial Intelligence, Zhejiang Lab, Hangzhou, China

*Correspondence to：

Shuang Wang*

Department of Neurology and Epilepsy Center, Second Affiliated Hospital, School of Medicine, Zhejiang University, Hangzhou 310009, China.

E-mail: wangs77@zju.edu.cn.

Dongping Yang*

Research Center for Augmented Intelligence, Research Institute of Artificial Intelligence, Zhejiang Lab, Hangzhou 311100, China.

E-mail: dpyang@zhejianglab.com.

Running title: ictal harmonic pattern in focal epilepsy

Key Words: harmonic pattern; ictal EEG; epileptogenic zone; nonlinear phenomena; epilepsy surgery.

Introduction

The epileptogenic zone (EZ), characterized as the site of primary organization of ictal discharge, pertains to the areas of excessive synchronization at seizure onset.[1] The completeness of EZ removal plays a crucial role in determining the surgical outcome for drug-resistant focal epilepsy. Intracranial electroencephalography (iEEG) offers the highest precision for EZ localization, especially for magnetic resonance imaging (MRI)-negative epilepsy.[2] At present, visual inspection constitutes a predominant method for clinical analyses of iEEG. Ictal patterns observed on iEEG exhibit significant heterogeneity in terms of onset morphology, evolution and propagation, suggesting a complex, highly dynamic and individualized nature of ictal network.[3] Among individuals who undergo iEEG evaluation followed by resective surgery, approximately 50-70% of the patients ultimately achieve prolonged seizure freedom.[4,5] The overall outcome of resective epilepsy surgery in focal epilepsy remains unsatisfactory, even among individuals with a focal onset pattern on iEEG.

In recent decades, many quantitative EEG methods have been developed to enhance the definition of EZ, complementing traditional visual inspection.[6] Examining interictal high frequency oscillations in conjunction with spikes on wide-band EEG recordings has been proved to be valuable for delineating the boundaries of EZ.[7-9] In studies focusing on ictal EZ markers, the majority of methods utilize fast activity (FA) either alone or in combination with other features.[10-13] The presence of focal ictal fast activity has been consistently associated with favorable surgical outcomes in neocortical epilepsy.[14] The epileptogenic index, which assesses alterations in the energy ratio between fast activity, predominantly in the gamma

range, and slow activity occurring at the early onset of a seizure in a specific region, offers a quantitative measurement for the epileptogenic network.[10] Epileptogenicity mapping can visualize such ictal EEG changes in energy ratio using statistical parametric mapping software.[11] Additionally, analyzing alteration in functional connectivity of the ictal low-voltage fast activity (LVFA) also provides complementary information for EZ localization.[15,16] Nevertheless, these methods typically rely on measuring fast activity exceeding 30 Hz, and may not be as efficient for slower EEG onset patterns, which constitute 20-30% of common onset patterns observed on iEEG.[17-19] Currently, efforts are ongoing to optimize ictal biomarkers of the EZ.

There has been a proposal for the concept of EEG fingerprints as ictal markers for the EZ, utilizing a carefully chosen cohort.[20,21] It encompasses three concurrent features within specific cortical regions: pre-ictal spiking, multiple-band fast activity, and simultaneous low-frequency suppression. One key finding is that the structural property of the ictal fast activity is as important as its powers. On time-frequency maps (TFM), the ictal fast activity consists of multiple narrow bands rather than broad-band activity. Notably, the identified narrow band activity mainly contains gamma or ripple oscillations and, at times, extends to beta or even alpha oscillations. The phenomenon of ictal narrow band activities may be prevalent in focal epilepsy and warrants further investigation.

In this study, we thoroughly investigate the spectral properties of ictal iEEG in focal epilepsy, with an aim to better clarify the clinical relevance of multi-band fast activity for EZ localization. We identified a unique and common spectral structure termed the “harmonic

pattern" (H pattern), characterized by multiple equidistant, high-density bands with varying frequencies over time. The characteristics of the initial H pattern and its clinical significance were examined in a cohort of individuals with focal epilepsy who underwent iEEG evaluation. Our findings indicate that the H pattern encapsulates biological information important for EZ localization. This is underscored by the correlation between the resection of the area expressing this feature and the surgical outcome. The H pattern observed on ictal EEG is not an isolated phenomenon; similar harmonic patterns harboring biological significance can be observed in other aspects of clinical neurophysiology. Moreover, we further delved into the mechanism responsible for the generation of the H pattern through nonlinear analysis.

Methods

Patients and stereo-electroencephalography evaluation

We conducted a review of consecutive patients with drug-resistant focal epilepsy who underwent stereo-electroencephalography (SEEG) evaluation followed by resective surgery at our epilepsy center between January 2014 and April 2021. All patients were monitored for more than two years after surgery. A comprehensive assessment was undertaken, encompassing a detailed medical history, neuropsychological testing, neuroimaging examination, and scalp video-EEG recordings. This study was approved by the Medical Ethics Committee of the Second Affiliated Hospital, Zhejiang University School of Medicine (Study No. 2020-910). SEEG was performed using intracerebral multiple-contacts electrodes, with contacts that were 2 mm in length, 0.8 mm in diameter, and 1.5 mm apart. SEEG signal

was recorded by EEG systems with 256 channels (Nihon Kohden) or 128 channels (Xltek, Natus, Ontario, Canada) at a sampling rate of 1000 or 2000 Hz. Pre-implantation MRI and post-implantation computed tomography (CT) were co-registered to locate each contact anatomically along each electrode trajectory.

EEG data were reviewed on bipolar montage. Only contacts within the grey matter were selected. The seizure onset pattern (SOP) was assessed on the earliest involved electrodes. As previously described,[8,15,22] the SOZ was defined as the area unequivocally showing the earliest change on iEEG, and early propagation zone (PZ) as the area showing a rapid spread of ictal activity within 3-5 seconds of seizure onset. Other brain regions were classified as other zone (OZ). The SOP, SOZ, PZ and OZ were independently defined by two clinical neurophysiologists. In the event of inconsistencies, discussions would be held with a third epileptologist to reach a consensus.

Surgical plans were devised by a multidisciplinary team, independent of the parameters considered in this study. After surgery, preoperative MRI and postoperative CT were integrated to identify precise borders of the resection. The electrode contacts located on resection margins or in disconnected tissues were defined as removed contacts. Surgical outcomes were assessed at the most recent follow-up based on Engel's classification. Surgical outcomes were classified as Engel Ia (seizure free, SF) and Engel >Ia (not seizure free, NSF).

Quantitative EEG analysis

Identification of Harmonic patterns

All analyses were conducted using bipolar signals recorded from artifact-free channels. For each seizure, a 110-second window of SEEG data was extracted: 10 s before and 100 s after the seizure onset, and another 110 s-epoch of SEEG data was also collected (> 2 min before the seizure onset) as a statistical baseline. Morlet wavelet transform analysis was used to generate TFM and subsequently validated using the multitaper method. Both methods used linear spacing in the frequency range of 1 to 300 Hz, with an interval of 1 Hz. The TFM of seizure was normalized by the baseline data, where the power at each frequency was divided by the corresponding baseline power (for methodological details, see Grinenko et al., 2018).[20]

The H pattern was identified based on the following features: multiple equidistant high-density, narrow bands with changing frequency over time (Fig. 1C). The frequency bands of the H pattern for each pair of channels, ranging from low to high, were denoted as the first (f_{1st}), second (f_{2st}), third frequency band (f_{3st}), and so forth. At a specific time point, the difference between two adjacent frequency bands was defined as the frequency interval, which is equal to the fundamental frequency (f). The frequencies of narrow bands fall around the multiples of the fundamental frequency. The minimal and maximal frequencies were determined at the peaks of the first and last frequency bands, respectively. Typically, this minimal frequency was equal to the fundamental frequency. The parameters of the H pattern, including minimal/maximal frequency and start/end time, were extracted using Brainstorm software. For one patient, the H pattern was usually consistent in habitual seizures, and we

randomly selected one seizure for analysis. In cases where several H patterns occurred consecutively within a single seizure, only the initial pattern was chosen for analysis.

To further identify channels exhibiting the dominant H pattern, a threshold of Q3 was set, represented as the upper quartile (75th percentile of data distribution) of the total band number:

$$Q3 = (n + 1) \times 3/4, \quad (1)$$

where n is the highest band number in each individual. Any channel with a band number of the H pattern exceeding this threshold would be designated as a “dominant-H pattern” (*d*H pattern) channel; otherwise it was labeled as a "non-dominant H pattern” (non-*d*H pattern) channel.

The correlation between removal of the region expressing *d*H pattern or SOZ and the postoperative outcome was analyzed. Resection ratio was calculated as the number of channels with the events included within the resection over the total number of channels where the events were observed.[8] A value of 1 indicates complete removal of the events, while a value of 0 represents complete non-removal.

Nonlinear analysis of H pattern

Since TFMs are generated by Morlet wavelet transforming the detrended SEEG signals, all information and features, such as the H pattern can be traced back to their waveshapes. Generally, the generation of harmonics can be ascribed to various factors, including nonlinear effects (e.g., impulses in a signal, nonsinusoidal waveshape distortion, etc.) and the

intermodulation of different frequencies. From a physic standpoint, the primary source of harmonic generation arises from nonlinear effects. For instance, as illustrated in Supplementary Fig. 2-3, the H pattern can be generated through various nonlinear transformations of a single frequency sinusoidal oscillation, leading to nonsinusoidal waveshapes.

The identification of the nonsinusoidal waveshapes in the SEEG signals, which account for the H pattern, was crucial for understanding the neural mechanism underlying the generation of the H pattern. To achieve this, the original SEEG signals were carefully analyzed. Initially, the signals underwent detrending using the smoothing method 'loess' in MATLAB to transform the wave's oscillations around a zero-valued baseline, thereby separating them into troughs and peaks. Subsequently, a sinusoidal wave with a single frequency was used to fit each trough and peak. Finally, specific nonsinusoidal waveshape distortion can be investigated and identified for each H pattern by comparing the frequencies of troughs and peaks, along with the primary component of the original signal, as elaborated in Fig. 5-6.

Bicoherence and cross-frequency amplitude-amplitude coupling analysis of H pattern

A harmonic structure can also arise from the intermodulation of different frequencies. In a phase-amplitude coupled (PAC) signal, the phase coupling of the modulation frequency (f_m) to the carrier frequency (f_c) leads to the emergence of amplitude-modulated side-peaks, which

typically manifest as the carrier frequency plus or minus the modulation frequency, i.e., (f_c ± f_m). If f_m = f_c - f_m, similar harmonic results (f_m, $2f_m$, $3f_m$) can be obtained.

To differentiate between the harmonic structures resulting from PAC and nonlinear effects manifested in the nonsinusoidal waveshapes, we utilized the bicoherence method and cross-frequency amplitude-amplitude coupling (AAC). These methods are commonly employed to characterize nonlinearity in dynamical system and dissociate the harmonic and non-harmonic PAC of EEG or magnetoencephalographic signals.[23] The relative strength and number of bicoherence and AAC peaks enables the dissociation of the harmonic structures due to PAC and nonlinear effects: bicoherence with more than two harmonic peaks denotes the presence of nonlinear effects. Moreover, the bicoherence and AAC between the fundamental frequency and its harmonics also indicate nonlinear effects, particularly when the bicoherence is strongest for identical f_1, and f_2 at the fundamental frequency.[23]

Bicoherence can be estimated according to the following formula with the normalization factor: [24]

$$\mathrm{b}(f_1, f_2) = \frac{|\sum_n \mathrm{F}(f_1)\mathrm{F}(f_2)*\mathrm{F}(f_1+f_2)|}{\sum_n |\mathrm{F}(f_1)\mathrm{F}(f_2)*\mathrm{F}(f_1+f_2)|} \quad (2)$$

where b(f_1, f_2) describes the phase coupling degree among three waves with a frequency of f_1, f_2, and $f_1 + f_2$, respectively, with a near-one value denoting strong coupling but a near-zero value denoting weak or even no coupling; F(f) is the Fourier transform of the signal, and * denotes the complex conjugate.

AAC can be estimated through the Pearson correlation coefficients between the amplitude time-series of two filtered time series at frequencies f_1 and f_2, respectively, which were obtained through Hilbert transformation.

In our study, bicoherence and AAC values were calculated for all frequency pairs (0-250 Hz, 0.25 Hz intervals), resulting in the wavelet bicoherence and AAC matrix. Each element, (f_1, f_2), represents the bicoherence and AAC values at the bifrequency pair (f_1, f_2), where $0 \leq f_1$, $f_2 \leq 250$ Hz. To ensure statistical significance, 100 surrogate datasets were generated using phase randomization, preserving spectral content and linear properties. A 99% statistical threshold was defined as mean plus two standard deviations (SD) of surrogated bicoherence or AAC estimates at each frequency pair. Only values above the threshold were considered significant for further analysis.

To facilitate statistical analyses, we defined six regions of interest (ROIs) in the bicoherence frequency map, representing all potential intersections of the first three frequency bands (Fig. 7C). We did not consider a higher number of frequency bands because the majority of H pattern channels have no more than three frequency bands. A total of 10 representative patients from five brain regions (temporal, frontal, parietal, occipital, and opercular/insular; 2 for each region) were selected for statistical analysis.

Statistical analysis

SPSS 24.0 software was used for statistical analysis. All continuous variables were first tested using a homogeneity test for variance and a test of normality. According to the results,

normal variables were presented as mean ± SD; and non-normal variables were reported as medians with interquartile ranges. Categorical variables were displayed as frequencies. Comparisons between two groups were made using Student's t tests or nonparametric Mann-Whitney U tests, and comparisons among three groups were analysed with one-way analyses of variance (ANOVAs) or nonparametric Kruskal-Wallis tests. Pearson's chi-square or Fisher's exact tests were used for categorical variables. Multivariate logistic regression was used to control for potential confounding factors when comparing *d*H pattern resection ratio between the two groups. A *P* (Bonferroni adjusted for multiple testing) value < 0.05 was considered statistically significant.

Results

Patients and iEEG evaluation

We examined SEEG data from all patients who were evaluated with SEEG between January 2014 and April 2021 (*n* = 80). Three patients were excluded due to insufficient clinical and EEG information, and another seven were excluded because of a non-localizable seizure onset origin. Among the 70 patients who were included, all seizures were classified into six seizure onset patterns (Fig. 1A):

Pattern 1, 36 cases with preictal spikes/sharps/polyspikes following fast activity > 14 Hz;

(a) Pattern 1.1: LVFA, amplitude < 30 μV;

(b) Pattern 1.2: high-voltage fast activity (HVFA), amplitude ≥ 30 μV.

Pattern 2, 10 cases with slow wave/DC shift followed by LVFA;

Pattern 3, 12 cases with spikes activity;

Pattern 4, seven cases with LVFA;

Pattern 5, three cases with beta activity;

Pattern 6, one case with delta-brush.

After a follow-up period of 35.5 ± 21.3 months, 48 patients (68.6%) achieved seizure freedom.

We reviewed TFM during the ictal periods in the 70 patients, fifty-seven patients presented with at least one H pattern, and the other 13 patients lacked of discernable H pattern. Notably, without TFM, direct visual inspection could not differentiate the EEG segments harboring H patterns from the counterparts without H-patterns. The H patterns could occur at different stages of the ictal phase, and their ictal SOPs could be all patterns except delta-brush (Fig. 1A-C). The EZ fingerprint, as defined by Grinenko et al's methods, was observed in 25 out of the 70 patients (35.7%).

No difference was found between the H pattern and non-H pattern groups in terms of SOP (P = 0.095, Fisher exact test), lobar origin (P = 0.475, Fisher exact test), presence of MRI lesion (85.9 % versus 76.9%, P = 0.416, Fisher exact test) or seizure freedom (68.4 % versus 69.2 %, P = 1.000, Fisher exact test). The most prevalent pathological finding in both groups was focal cortical dysplasia II (FCD II) (49.1 % versus 38.5 %, Fisher exact test). In the end, 57 patients (81.4%) were included in the subsequent analysis of the H pattern (Table 1).

Among the 57 patients recorded with H pattern, there were 31 males and 26 females. The mean age at epilepsy onset was 10.4 ± 8.5 years. The mean age of the patients at surgery was

23.6 ± 12.3 years. The mean number of contacts per patient was 94.7 ± 29.1. Forty-nine patients (85.9 %) exhibited identified or subtle lesions on MRI. The most common seizure origins were the frontal and temporal lobes, with FCD II being the most prevalent pathological finding (49.1%). At the final follow-up, 39 patients (68.4%) achieved seizure freedom (Table 1). No differences in various features were found between SF and NSF groups, except for pathological findings, in which there were significant differences between FCD II and gliosis/nonspecific findings.

Classification of H pattern

The initial H pattern emerged 18.1 ± 20.5 s after the ictal EEG onset on TFM. Its onset time was not confined to the early stage of seizure evolution but occasionally extended to the late stage of seizures (Fig. 1C). The H pattern was specifically embedded in two types of EEG segments: fast activity > 25 Hz and irregular polyspikes > 5 Hz. Consequently, H patterns were classified into two types: FA-H pattern and PS-H pattern (Fig. 2A). For the initial H pattern observed, their proportions were close (FA-H pattern, 30/57; PS-H pattern, 27/57). A lower number of bands (P = 0.006, nonparametric Mann-Whitney U test) and a higher frequency interval (P < 0.001, nonparametric Mann-Whitney U test) were found for FA-H pattern compared with PS-H pattern. Additionally, in the FA-H pattern, both the start time (P = 0.004, nonparametric Mann-Whitney U test) and the end time (P = 0.015, nonparametric Mann-Whitney U test) were earlier than those in the PS-H pattern. The minimal frequency (P < 0.0001, nonparametric Mann-Whitney U test) and maximal frequency (P = 0.021,

nonparametric Mann-Whitney U test) were higher (Fig. 2B). In all H patterns, the frequencies of bands varied over time, exhibiting upwards, downwards, or were bell-shaped before eventually disappearing.

Spatial distribution of H pattern

The H pattern commonly occurred in the SOZ, PZ and sometimes in the OZ at very close time points, displaying nearly the same frequency interval, even when these regions were remotely separated (Fig. 3C). The end time and minimal/maximal frequencies of the H pattern did not differ across regions. Sometimes the H pattern extended to the ipsilateral thalamus, occurring concurrently with the cortical regions and demonstrating the same frequency interval (Supplementary Fig. 1).

The proportion of contacts displaying the H pattern in each region decreased in the order from SOZ, PZ to OZ (SOZ vs PZ, $P < 0.001$; SOZ vs OZ, $P < 0.001$; PZ vs OZ, $P = 0.004$, nonparametric Kruskal-Wallis tests, after Bonferroni correction). The highest number of bands was in the SOZ (SOZ vs PZ, $P = 0.014$; SOZ vs OZ, $P < 0.001$, PZ vs OZ, $P = 0.012$, nonparametric Kruskal-Wallis tests, after Bonferroni correction, Fig. 3C).

Dominant H pattern and surgical outcome

The H pattern in most SOZ showed the highest number of bands (Fig. 3C). To identify H pattern regions potentially marking epileptogenicity, we defined the *d*H pattern regions using Q3 as a threshold in each patient. Patients in the SF group had a significantly larger resection

proportion of areas expressing the *d*H pattern compared to those in the NSF group ($P < 0.001$, nonparametric Mann-Whitney U test). No such difference was found in the SOZ ($P = 0.966$, nonparametric Mann-Whitney U test) (Fig. 4A). On multivariate analysis, after adjusting for potential confounders of pathology, presence of MRI lesion, and epilepsy duration, a complete resection of areas expressing the *d*H pattern was still significantly associated with a chance of seizure freedom (Fig. 4B).

EEG waveshapes accounting for H pattern

Analyzing the EEG waveshapes of *d*H and non-*d*H patterns for both types of H pattern revealed FA-H pattern can be generated by diverse waveshapes, including sharper troughs, sharp extended troughs and peaks, asymmetric waveshapes, and phase-locked high frequency amplitude, while PS-H pattern was caused by rhythmic pulses. In the subsequent analysis, we selected four cases exemplifying FA-H pattern and one case illustrating PS-H pattern for a detailed investigation.

The first case contributing to the FA-H pattern featured a waveshape characterized by sharper troughs, as illustrated in Fig. 5, left panel. The original signals, detrended signals and corresponding TFMs with clear harmonic patterns (Fig. 5A and D) revealed higher power of harmonic components but lower power of the primary component in the *d*H pattern compared to those in the non-*d*H pattern. The sinusoidal waves were then used to fit troughs and peaks, along with the corresponding fitted periods and TFMs (Fig. 5B and E). The strong harmonic components in the *d*H pattern were due to the sharp troughs (Fig. 5B middle and

demonstration in Supplementary Fig. 3A), while the weaker harmonic components in the non-*d*H pattern were results of the period fluctuation of both troughs and peaks (Fig. 5E, middle). The point was further supported by the distribution of fitted periods for both troughs and peaks, as well as their consequent pairs (Fig. 5C and F).

The second case demonstrated the waveshape with sharp extended troughs and peaks (Fig. 5G, right panel). The harmonic components in the low frequency region (< 150 Hz) were dominated by the 1st and 3rd orders of the primary frequency (Fig. 5G bottom). The results indicated that the sinusoidal waves were sharper and had shorter periods than the primary period of the EEG signal in the *d*H pattern (Fig. 5H, middle). Correspondingly, the sharp sinusoidal waves in the *d*H pattern are extended with more than half of the primary period, as demonstrated in Fig. 5I bottom, where the ratio of durations of both troughs and peaks over the primary period was much larger than half, as shown in the simple case in Supplementary Fig. 3B. In contrast, this effect was much reduced in the non-*d*H pattern (Fig. 5L bottom).

The third case was comprised of asymmetric waveshape (Fig. 6, left panel). The results showed that the *d*H pattern exhibited stronger harmonic components compared to those of the non-*d*H pattern. The signals fitted with sinusoidal waves also demonstrated much stronger harmonic components in the *d*H pattern in comparison with those in the non-*d*H pattern (Fig. 6B and E, bottom). This could be explained by another feature: an asymmetric waveshape with longer trough-to-peak durations than peak-to-trough durations (Fig. 6C and F), as demonstrated by a simple case presented in Supplementary Fig. 3C.

The fourth FA-H pattern was similar to that in the previous study,[25] as illustrated by EEG of both *d*H pattern and non-*d*H pattern in Supplementary Fig. 4. The *d*H pattern exhibited features resembling those in the ictal core with robust high frequency activity (80-150 Hz), while the non-*d*H pattern displayed similar features to those in the penumbra of Weiss's study.[25] The stronger harmonic components in the *d*H pattern were attributed to an elevated high frequency activity at the peak of the lower frequency rhythm (4-30 Hz). This kind of phase-locked high frequency amplitude occurred at the onset of LVFA, preceding the emergence of the clear H pattern (Supplementary Fig. 4).

The waveshape contributing to the PS-H pattern was characterized by sharp rhythmic pulses (Fig. 6, right panel). The key distinction between the *d*H pattern and non-*d*H pattern resided in the rhythmic pulses, the elimination of which markedly diminished the power of harmonic components in *d*H pattern (Fig. 6H), and rendered the remaining EEG signals of the *d*H pattern similar to those of the non-*d*H pattern (Fig. 6H and K). The harmonic components could be further diminished by fitting sinusoidal waves to troughs and peaks (Fig. 6I and L). Furthermore, the remaining EEG signals of the *d*H pattern exhibited a larger amplitude than those of the non-*d*H pattern, indicating that the region of the non-*d*H pattern was driven by activities in the region of the *d*H pattern. The sharp rhythmic pulses in the *d*H pattern might be filtered out during spatiotemporal signal propagation.

Differentiating between the harmonic structures resulting from PAC and nonlinear effects

In 10 representative cases, the results indicate that the observed harmonic pattern was attributed to nonlinear effects rather than PAC (Fig. 7): the presence of multiple peaks of bicoherence and AAC between the fundamental frequency and its harmonics. The mean of the maximum bicoherence values in both the *d*H pattern and the non-*d*H pattern were the strongest for identical f_1 and f_2 at the fundamental frequency (ROI1).

Following this, we conducted a comparison of the mean maximum bicoherence values between the *d*H pattern and the non-*d*H pattern. The outcomes revealed that all ROIs demonstrated higher bicoherence in the *d*H patterns compared to the non-*d*H patterns (nonparametric Mann-Whitney U test). This suggests that the nonlinear effects are stronger in *d*H pattern than in non-*d*H pattern (Fig. 7D).

Discussion

As a distinct feature on TFM recorded in ictal SEEG signals, H pattern and its correlation with EZ were systematically investigated in this study. H pattern was commonly present in most patients with various EEG onset patterns, either during early or late seizure propagation.[25] Moreover, despite substantial variations in the morphology and features of H pattern across individuals, each patient exhibited highly uniform pattern for all habitual seizures, suggesting that it represents an individualized property of epileptogenic network. The H pattern was found to be spatially co-localized within the epileptic zones of SOZ and PZ, showing the highest numbers of bands in these regions. Importantly, a complete resection of cortical regions expressing dominant H patterns, rather than the SOZ, emerged as an

independently predictor of seizure freedom following resective surgery in our cohort of focal onset epilepsy. This underscores the potential of H pattern dominancy as a promising and universal ictal marker for identifying the EZ. Additionally, our study revealed that H pattern can be associated with diverse waveshapes, reflecting nonlinear features in the seizure. This diversity suggests various underlying neuronal mechanisms with clinical significance, distinct from intermodulation of frequencies or methodological artifacts. When H patterns occurred in different cortical regions, a consistent fundamental frequency was observed, indicating a pivotal stage of inter-regional synchronization during seizure propagation. The analysis of H pattern not only yields crucial insights into the dynamics of ictal neural activity but also offers valuable information about the EZ.

Many quantitative methods have been developed to supplement visual EEG analysis and objectively delineate the EZ. These approaches typically involve assessing the energy of ictal fast activity. The epileptogenicity index is calculated as the energy ratio between the fast frequencies and slow frequencies.[10] David et al. (2011) sought to pinpoint the EZ by focusing on the maximal frequency of FA during the early spread of seizures.[11] Gnatkovsky et al. (2014) discovered that the EZ could be characterized by combined features at seizure onset, including ictal fast activity at 80-120 Hz, associated with a polarizing shift and EEG flattening.[13] Our study reinforces the relevance of the spectral properties of ictal fast activity in defining the EZ. Some of the FA-H patterns observed in our study bear resemblance to narrow band fast activity with suppressed lower-frequency activity, as defined in EEG fingerprint studies.[20] Furthermore, this highly-structured spectral feature was also observed

during later seizure propagation for PS-H patterns, even in seizures absent of initial fast activity. Our findings broaden the scope of narrow band fast activity defined in study of EEG fingerprints, proposing the possibility of expanding the time window for defining the EZ using ictal EEG. In our study group, the sensitivity for detecting EEG fingerprint was 0.357. Notably, the ictal H pattern was prevalent, and its occurrence was unrelated to the initial fast activity during seizure onset. In future, analyzing the ictal H pattern on TFM emerges as a practical method to complement other quantitative methods in precisely defining the EZ.

The FA-H pattern and PS-H pattern manifested during different stages of seizure evolution. In vivo and brain slice unit recording studies reveal that diverse neuronal populations play specific roles at different stages of seizure evolution. A typical partial seizure, as captured with depth electrodes, commences with either fast activity or “hypersynchronous” potentials, followed by irregular spiking, and eventually evolves into rhythmic bursts.[26] Compelling evidence indicates that the occurrence of fast activity is underpinned by a significant activation of inhibitory interneurons, coupled with a transient shutdown of excitatory cells.[27-32] Consequently, irregular spiking is linked to a decrease in inhibitory interneuron firing and an increase in excitatory interactions among excitatory neurons. During the terminal phase, bursting activity is marked by augmentation of both interneurons and excitatory neurons.[33] Consequently, FA-H pattern may be predominantly influenced by inhibitory interneurons, while the PS-H pattern is characterized by a more substantial involvement of excitatory neuron firing.

Neural oscillations represent a prominent feature of brain recordings and are frequently associated with both normal and pathological behaviors, including sleep, perception, cognition, and epileptic seizures.[34,35] In spectral analysis, it is a common practice to filter signals into specific frequency bands of interest. This approach defaults to treating the EEG signal as a sine wave and applies smoothing, but may alter or eliminate subtle features of the waveshape. Increasing evidence suggests that neural oscillations are often non-sinusoidal. Characteristics of non-sinusoidal signals, such as general shape, sharpness, and rise-to-decay asymmetry,[36,37] are likely pertinent to the underlying physiology.[37,38] In this study, we demonstrated that distinct waveshapes can explain the observed H pattern in various patients, allowing for the discrimination of *d*H pattern from non-*d*H pattern. In the case of FA-H pattern, the harmonics in *d*H pattern arise from sharper troughs or/and peaks, asymmetric waveshapes, and even the phase-locked high frequency amplitudes at specific phases (negative or positive peaks) of the low-frequency rhythm. For PS-H pattern, the harmonics in *d*H pattern originate from a more consistent waveshape, primarily the sharp rhythmic pulses. As mentioned earlier, the synchronization of interneurons is implicated in the generation of the FA-H pattern, while that of excitatory neurons is associated with the PS-H pattern. During the onset of FA, the synchronization level of interneurons undergoes changes in tandem with the surrounding ion concentrations, notably the extracellular potassium $[K^+]_o$, influenced by the increasing hyperactivity of interneurons. This coevolving system, characterized by neuronal synchronization and rapidly changing ion environments, is replete with intricate nonlinear interactions. These interactions underlie the emergence of various brain oscillations,

including the H pattern elucidated in this study. In summary, our findings unveil the influence of nonlinear phenomena on EEG dynamics during seizures, enriching our grasp of the ictal network. The potency of these non-linear interactions orchestrates specific physiological and pathological functions and can serve as a marker for epileptogenicity. Further research is imperative to elucidate the cellular and dynamic mechanisms corresponding to various waveshapes responsible for the observed H pattern. In contrast, in the case of PS onset, the synchronization of excitatory neurons is more straightforward, leading to a more consistent observed waveshape that accounts for the PS-H pattern across different patients.

Harmonic phenomena have a well-established presence in fields of sonics and electric circuits.[39-41] Similarly, such harmonic phenomena can be observed in EEG or local field potential signals, potentially linked to specific brain functional states.[42,43] For instance, during NREM sleep, sleep spindles exhibit harmonic phenomena, with parameters changing in accordance with sleep stages, reflecting functional alterations in the thalamocortical reverberant network.[44] Additionally, steady-state visual evoked potentials, indicative of responses in the parietooccipital cortex to periodic light stimulation, manifest harmonics and subharmonics corresponding to the frequency of stimulus.[45] Nevertheless, harmonic phenomena have not garnered significant attention in the field of epilepsy, despite being commonly demonstrated in ictal EEG recordings from both animal models and patients.[46 47,48] The concept of a “chirp signal” in ictal iEEG, characterized by varying frequency content over time, was identified as co-localized with SOZ and exhibited striking similarities to the H pattern.[48] This early study involved a small cohort of six patients with focal epilepsy, and the

parameters of the chirp signals were not thoroughly explored. Currently, the biological significance of harmonic phenomena in epilepsy and the mechanism behind their generation remain poorly understood. Moreover, they are often dismissed as artifacts in clinical or experimental studies. However, we posit that harmonic features harbor localizing information about the neural dynamics of seizures. Our study suggests a potential linkage to diverse nonlinear transformations of sinusoidal waves, thus being rooted in various underlying neuronal mechanisms. This complex and diverse mechanism exhibits a common feature, H pattern, indicating it could serve as a unique window for exploring the nature of epilepsy and its neural correlations.

In our study, the H pattern shows narrowband oscillations rather than broadband oscillations. These narrowband oscillations signify the synchronized firing of neuronal populations in the cortex.[49-51] We observed that the fundamental frequencies of the SOZ, PZ and OZ were identical during the occurrence of H pattern, indicating synchronized neural firing across these regions. Remarkably, this cross-regional synchronization in fundamental frequency can spread to very remote areas, including contralateral cortical regions or even the ipsilateral thalamus. The H pattern represents a distinctive stage of seizure propagation. Particularly, the *d*H pattern exhibits elevated bicoherence values, indicating a stronger nonlinear effects. Our approach builds upon prior efforts that employed bicoherence to facilitate the recognition and description of harmonic structures. Our results demonstrate that bicoherence can not only quantify nonlinear features but also aids in differentiating between the *d*H pattern and non-*d*H pattern.

The study has several limitations. First, it relies on a cohort recruited from a single center, and its cellular mechanisms cannot be explored. Secondly, due to the heterogeneous morphology of H patterns across subjects and the current lack of automated identification, their visual recognition inherently subjective to personal experience, introducing subjectivity. Moreover, multiple H patterns may occur in the same seizure, and only the first occurrence was analyzed in this study. Further investigation is warranted for cases where H patterns appear consecutively. Thirdly, the threshold Q3 used to define the dominant H pattern. A patient-specific approach for defining dominancy in H patterns may be necessary in future studies.

Conclusion

Our study defines a common and distinctive ictal spectral feature known as the H pattern, which may be associated with rhythmic synchronization of intense neuronal firing of underlying specific neuronal populations. The H pattern imparts unique information about ictal neural dynamics and offers novel insights into the EZ. Our data also provides evidence supporting an elongated time-window for measuring the EZ using quantitative EEG.

Data availability

The data that support the findings of this study are available upon reasonable request from the corresponding author. The data are not publicly available to protect the privacy of research participants.

Funding

This work was supported by the National Natural Science Foundation of China (grant numbers: 82171437 and 82301636) and the Natural Science Foundation of Zhejiang Province (grant no. LD24H090003 and LY24H090004).

Competing interests

The authors report no competing interests.

Supplementary material

Supplementary material is available at *Brain* online.

References

1. Bancaud J, Angelergues R, Bernouilli C, et al. Functional stereotaxic exploration (SEEG) of epilepsy. *Electroencephalogr Clin Neurophysiol.* 1970;28(1):85-86.

2. Jin B, So NK, Wang S. Advances of Intracranial Electroencephalography in Localizing the Epileptogenic Zone. *Neurosci Bull.* 2016;32(5):493-500.

3. Devinsky O, Vezzani A, O'Brien TJ, et al. Epilepsy. *Nature reviews Disease primers.* 2018;4:18024.

4. Sivaraju A, Hirsch L, Gaspard N, et al. Factors Predicting Outcome After Intracranial EEG Evaluation in Patients With Medically Refractory Epilepsy. *Neurology.* 2022;99(1):e1-e10.

5. He C, Chen C, Yang Y, et al. Clinical Characteristics and Prognostic Significance of Subclinical Seizures in Focal Epilepsy: A Retrospective Study. *Neurol Ther.* 2022;11(2):763-779.

6. Frauscher B. Localizing the epileptogenic zone. *Current opinion in neurology.* 2020;33(2):198-206.

7. Frauscher B, Bartolomei F, Kobayashi K, et al. High-frequency oscillations: The state of clinical research. *Epilepsia.* 2017;58(8):1316-1329.

8. Wang S, So NK, Jin B, et al. Interictal ripples nested in epileptiform discharge help to identify the epileptogenic zone in neocortical epilepsy. *Clin Neurophysiol.* 2017;128(6):945-951.

9. Wang S, Wang IZ, Bulacio JC, et al. Ripple classification helps to localize the seizure-onset zone in neocortical epilepsy. *Epilepsia.* 2013;54(2):370-376.

10. Bartolomei F, Chauvel P, Wendling F. Epileptogenicity of brain structures in human temporal lobe epilepsy: a quantified study from intracerebral EEG. *Brain.* 2008;131(Pt 7):1818-1830.

11. David O, Blauwblomme T, Job AS, et al. Imaging the seizure onset zone with stereo-electroencephalography. *Brain.* 2011;134(Pt 10):2898-2911.

12. Gnatkovsky V, Francione S, Cardinale F, et al. Identification of reproducible ictal patterns based on quantified frequency analysis of intracranial EEG signals. *Epilepsia.* 2011;52(3):477-488.

13. Gnatkovsky V, de Curtis M, Pastori C, et al. Biomarkers of epileptogenic zone defined by quantified stereo-EEG analysis. *Epilepsia.* 2014;55(2):296-305.

14. Wetjen NM, Marsh WR, Meyer FB, et al. Intracranial electroencephalography seizure onset patterns and surgical outcomes in nonlesional extratemporal epilepsy. *Journal of neurosurgery.* 2009;110(6):1147-1152.

15. Hu L, Xiong K, Ye L, et al. Ictal EEG desynchronization during low-voltage fast activity for prediction of surgical outcomes in focal epilepsy. *Journal of neurosurgery.* 2023;139(1):238-247.

16. Wilke C, Worrell G, He B. Graph analysis of epileptogenic networks in human partial epilepsy. *Epilepsia*. 2011;52(1):84-93.

17. Singh S, Sandy S, Wiebe S. Ictal onset on intracranial EEG: Do we know it when we see it? State of the evidence. *Epilepsia.* 2015;56(10):1629-1638.

18. Lagarde S, Buzori S, Trebuchon A, et al. The repertoire of seizure onset patterns in human focal epilepsies: Determinants and prognostic values. *Epilepsia.* 2019;60(1):85-95.

19. Balatskaya A, Roehri N, Lagarde S, et al. The "Connectivity Epileptogenicity Index " (cEI), a method for mapping the different seizure onset patterns in StereoElectroEncephalography recorded seizures. *Clin Neurophysiol.* 2020;131(8):1947-1955.

20. Grinenko O, Li J, Mosher JC, et al. A fingerprint of the epileptogenic zone in human epilepsies. *Brain.* 2018;141(1):117-131.

21. Li J, Grinenko O, Mosher JC, Gonzalez-Martinez J, Leahy RM, Chauvel P. Learning to define an electrical biomarker of the epileptogenic zone. *Hum Brain Mapp.* 2020;41(2):429-441.

22. Wang MY, Wang J, Zhou J, et al. Identification of the epileptogenic zone of temporal lobe epilepsy from stereo-electroencephalography signals: A phase transfer entropy and graph theory approach. *NeuroImage Clinical.* 2017;16:184-195.

23. Giehl J, Noury N, Siegel M. Dissociating harmonic and non-harmonic phase-amplitude coupling in the human brain. *Neuroimage*. 2021;227:117648.

24. Bullock TH, Achimowicz JZ, Duckrow RB, Spencer SS, Iragui-Madoz VJ. Bicoherence of intracranial EEG in sleep, wakefulness and seizures. *Electroencephalography and clinical neurophysiology.* 1997;103(6):661-678.

25. Weiss SA, Banks GP, McKhann GM, Jr., et al. Ictal high frequency oscillations distinguish two types of seizure territories in humans. *Brain.* 2013;136(Pt 12):3796-3808.

26. de Curtis M, Gnatkovsky V. Reevaluating the mechanisms of focal ictogenesis: The role of low-voltage fast activity. *Epilepsia.* 2009;50(12):2514-2525.

27. Velazquez JL, Carlen PL. Synchronization of GABAergic interneuronal networks during seizure-like activity in the rat horizontal hippocampal slice. *Eur J Neurosci.* 1999;11(11):4110-4118.

28. Köhling R, Vreugdenhil M, Bracci E, Jefferys JG. Ictal epileptiform activity is facilitated by hippocampal GABAA receptor-mediated oscillations. *J Neurosci.* 2000;20(18):6820-6829.

29. Ziburkus J, Cressman JR, Barreto E, Schiff SJ. Interneuron and pyramidal cell interplay during in vitro seizure-like events. *J Neurophysiol.* 2006;95(6):3948-3954.

30. Lasztóczi B, Nyitrai G, Héja L, Kardos J. Synchronization of GABAergic inputs to CA3 pyramidal cells precedes seizure-like event onset in juvenile rat hippocampal slices. *J Neurophysiol.* 2009;102(4):2538-2553.

31. Gnatkovsky V, Librizzi L, Trombin F, de Curtis M. Fast activity at seizure onset is mediated by inhibitory circuits in the entorhinal cortex in vitro. *Ann Neurol.* 2008;64(6):674-686.

32. Fujiwara-Tsukamoto Y, Isomura Y, Imanishi M, et al. Prototypic seizure activity driven by mature hippocampal fast-spiking interneurons. *J Neurosci.* 2010;30(41):13679-13689.

33. de Curtis M, Avoli M. Initiation, Propagation, and Termination of Partial (Focal) Seizures. *Cold Spring Harbor perspectives in medicine*. 2015;5(7):a022368.

34. Samarasinghe RA, Miranda OA, Buth JE, et al. Identification of neural oscillations and epileptiform changes in human brain organoids. *Nature neuroscience.* 2021;24(10):1488-1500.

35. Cole S, Voytek B. Cycle-by-cycle analysis of neural oscillations. *J Neurophysiol.* 2019;122(2):849-861.

36. Sherman MA, Lee S, Law R, et al. Neural mechanisms of transient neocortical beta rhythms: Converging evidence from humans, computational modeling, monkeys, and mice. *Proc Natl Acad Sci U S A.* 2016;113(33):E4885-4894.

37. Cole SR, Voytek B. Brain Oscillations and the Importance of Waveform Shape. *Trends Cogn Sci.* 2017;21(2):137-149.

38. Cole SR, van der Meij R, Peterson EJ, de Hemptinne C, Starr PA, Voytek B. Nonsinusoidal Beta Oscillations Reflect Cortical Pathophysiology in Parkinson's Disease. *J Neurosci.* 2017;37(18):4830-4840.

39. Schaefer MK, Kössl M, Hechavarría JC. Laminar differences in response to simple and spectro-temporally complex sounds in the primary auditory cortex of ketamine-anesthetized gerbils. *PLoS One.* 2017;12(8):e0182514.

40. Kanwal JS, Rauschecker JP. Auditory cortex of bats and primates: managing species-specific calls for social communication. *Frontiers in bioscience : a journal and virtual library.* 2007;12:4621-4640.

41. Ebadian H, Mohebbi M. Strong electric field enhancements in asymmetric metallic nanostructures and high-order harmonic generation. *Applied optics.* 2016;55(28):8035-8041.

42. Marceglia S, Foffani G, Bianchi AM, et al. Dopamine-dependent non-linear correlation between subthalamic rhythms in Parkinson's disease. *J Physiol.* 2006;571(Pt 3):579-591.

43. Coelli S, Tacchino G, Visani E, Panzica F, Franceschetti S, Bianchi AM. Higher order spectral analysis of scalp EEG activity reveals non-linear behavior during rhythmic visual stimulation. *J Neural Eng.* 2019;16(5):056028.

44. Abeysuriya RG, Rennie CJ, Robinson PA, Kim JW. Experimental observation of a theoretically predicted nonlinear sleep spindle harmonic in human EEG. *Clin Neurophysiol*. 2014;125(10):2016-2023.

45. Müller-Putz GR, Scherer R, Brauneis C, Pfurtscheller G. Steady-state visual evoked potential (SSVEP)-based communication: impact of harmonic frequency components. *J Neural Eng*. 2005;2(4):123-130.

46. Lévesque M, Salami P, Gotman J, Avoli M. Two seizure-onset types reveal specific patterns of high-frequency oscillations in a model of temporal lobe epilepsy. *J Neurosci*. 2012;32(38):13264-13272.

47. Lévesque M, Herrington R, Hamidi S, Avoli M. Interneurons spark seizure-like activity in the entorhinal cortex. *Neurobiol Dis*. 2016;87:91-101.

48. Schiff SJ, Colella D, Jacyna GM, et al. Brain chirps: spectrographic signatures of epileptic seizures. *Clin Neurophysiol.* 2000;111(6):953-958.

49. Fries P, Nikolic D, Singer W. The gamma cycle. *Trends Neurosci.* 2007;30(7):309-316.

50. G Bk. Rhythms of the brain. *New York: Oxford UP.* 2006.

51. Manning JR, Jacobs J, Fried I, Kahana MJ. Broadband shifts in local field potential power spectra are correlated with single-neuron spiking in humans. *J Neurosci*. 2009;29(43):13613-13620.

Figure legends

Figure 1 H patterns recorded in seizures with various ictal EEG onset patterns. (A) The six ictal onset patterns on SEEG: 1.1, preictal spikes/sharps/polyspikes followed LVFA; 1.2, preictal spikes/sharps/polyspikes followed HVFA; 2, slow wave/ DC shift followed by LVFA; 3, spikes activity; 4, LVFA; 5, beta activity; 6, delta-brush. **(B)** The percentage of patients presenting with certain EEG onset patterns that did or did not exhibit H pattern. The H pattern was present in all onset patterns except for the delta-brush. **(C)** EEG and corresponding TFM (top and middle) during seizures. The TFM shows the proposed 'harmonic pattern (H pattern)': multiple equidistant high-density, narrow bands with changing frequency over time. The initial H patterns presented at various seizure stages on TFM. The black double arrows in the red box mark the start time point of the H pattern. The power spectral density corresponding to the maximum frequency point of the H pattern (the black arrow) demonstrates an equidistant distribution of the frequency bands (bottom). The frequency intervals were 26, 27 and 16 Hz, respectively. LVFA: low-voltage fast activity; HVFA: high-voltage fast activity; TFM: time frequency map; Max Freq: maximal frequency; Min Freq: minimal frequency; f_{1st}: the first frequency band, f_{2st}: the second frequency band, f_{3st}: the third frequency band; f: fundamental frequency. Red star: seizure onset.

Figure 2 Two types of EEG segments harboring H pattern. (A) The H pattern is presented in fast activity (FA-H pattern) and irregular polyspikes (PS-H pattern). The power spectral density (bottom) at the maximum frequency point shows an equidistant distribution of the frequency bands. **(B)** Comparison of parameters between the FA-H pattern and PS-H pattern. The former has a fewer number of frequency bands (3 (4.25) vs 6 (8.5)), higher frequency interval (47.5 (56.75) vs 15 (20) Hz), earlier start (5.2 (18.19) vs 18.7 (17.2) s) and end (25.4 (28.3) vs 33.9 (11.7) s) time, and higher minimal (60 (54.7) vs 15(20) Hz) and maximal (193 (120.75) vs 126 (159) Hz) frequencies than the latter. *$P < 0.05$; **$P < 0.01$; ***$P < 0.001$. Max Freq: maximal frequency; Min Freq: minimal frequency.

Figure 3 Distribution of H pattern. (A) Anatomical distribution of the SOZ, PZ, and OZ in a patient (left panel). In this case, the SOZ is located in the precentral gyrus with early propagation to the postcentral gyrus. The right panel **(B)** shows the corresponding EEG recordings from the SOZ, PZ, and OZ, along with the observed H pattern. Red stars indicate seizure onset. **(C)** Comparison of parameters among the SOZ, PZ, and OZ in group data.

The distribution percentage of the H pattern decreases in the order of SOZ, PZ, and OZ. The SOZ exhibits the highest number of bands. *$P < 0.05$; **$P < 0.01$; ***$P < 0.001$. Max Freq: maximal frequency; Min Freq: minimal frequency; SOZ: seizure onset zone; PZ: early propagation zone; OZ: other zone.

Figure 4 Resection of dominant H pattern and surgical outcome. (A) Patients in the SF group had a significantly larger resection proportion of the dominant H pattern than those in the NSF group. No such difference was observed for the SOZ. *$P < 0.05$; **$P < 0.01$; ***$P < 0.001$. *d*H pattern: dominant H pattern. SOZ: seizure onset zone. **(B)** Multivariate logistic regression analysis. After adjusting for potential confounders, including pathology, lesional MRI, and epilepsy duration, a complete resection of areas showing the dominant H pattern was correlated with achieving seizure freedom.

Figure 5 Two representative illustrations of nonlinear analysis of *d*H and non-*d*H patterns in FA-H patterns. The left panel shows the first example: more harmonic components in *d*H pattern is attributed to sharper troughs of the FA waves compared to those in non-*d*H pattern. **A/D**: original SEEG signals in *d*H/non-*d*H patterns (top), detrended SEEG signals (middle), TFM (bottom); **B/E**: troughs (blue circles) and peaks (red stars) of FA signals (blue lines) in *d*H/non-*d*H patterns fitted by sin waves (red lines) respectively (top), with periods T of each wave shown at the middle layer, and TFM of the fitting waves at the bottom layer; **C/F**: histograms of periods (left) and trough period vs. peak period (right) of the fitted FA signals for *d*H/non-*d*H patterns. The right panel illustrates the second example: more harmonic components in the *d*H pattern is due to sharp extended troughs and peaks of the FA waves. **G/J**: original SEEG signals in *d*H/non-*d*H patterns (top), detrended SEEG signals (middle), TFM (bottom); **H/K**: troughs (blue circles) and peaks (red stars) of FA signals (blue lines) in *d*H/non-*d*H patterns fitted by sin waves (red lines) respectively (top), with periods T

of each wave shown at the middle layer, TFM of the fitting waves at bottom layer. As shown in the middle layer, both troughs (red stars) and peaks (blue circles) are sharp with shorter periods than the primary period (black dashed line) of the EEG signal of *d*H pattern; **I/L**: enlarged plots of detrended SEEG signals and sine fitting with troughs and peaks, whose durations over periods of sine wave are shown at the bottom layer. The sharp sine waves for both troughs and peaks in *d*H pattern extend for more than half of the primary period of the EEG signal in **I**. This indicates that the ratio of durations for both troughs and peaks over the primary period was much larger than half in **I**, at the bottom. The green dashed line in **A-B**, **D-E** and **G-L** represents the thresholds for extracting the periods of troughs and peaks, set as SD/2 for the *d*H pattern and SD/3 for the non-*d*H pattern. SD: standard deviation. FA: fast activity. FA is indicated as the region between two red vertical lines.

Figure 6 Two representative illustrations of nonlinear analysis of *d*H and non-*d*H patterns in FA-H pattern and PS-H pattern. The left panel shows the third example of FA-H pattern: stronger harmonic components in the *d*H pattern resulted from asymmetric waveshapes. **A/D**: original SEEG signals in *d*H/non-*d*H patterns (top), detrended SEEG signals (middle), TFM (bottom); **B/E**: troughs (blue circles) and peaks (red stars) of FA signals (blue lines) in *d*H/non-*d*H patterns fitted by sine waves (red lines) respectively (top), with periods T of each wave shown at the middle layer, and TFM of the fitting waves at the bottom layer; **C/F**: enlarged plots of detrended SEEG signals, where trough-to-peak (left blue triangle) and peak-to-trough (right red triangle) durations are compared at the bottom layer.

Green dashed lines in **A-B** and **D-E** are the same as those in Fig. 5. The region between two red vertical lines indicates the FA region. The right panel shows the example of PS-H pattern: More harmonic components in the *d*H pattern are due to the sharp rhythmic pulses of the PS waves, which do not exist in the non-*d*H pattern. **G/J**: original SEEG signals in *d*H/non-*d*H patterns (top), detrended SEEG signals (middle), and TFM (bottom); **H/K**: PS waves with/without sharp pulses in *d*H/non-*d*H patterns. Removing pulses of the PS waves in the *d*H pattern (top in **H**) results in similar waves in *d*H and non-*d*H patterns but with a larger wave amplitude (middle in **H**) in the *d*H pattern than that (top in **K**) in non-*d*H pattern. Similar TFM of PS waves without pulses in *d*H (bottom in **H**) and non-*d*H (bottom in **K**) patterns. **I/L**: sin wave fitting (black) further diminishes the harmonic components in both *d*H (bottom in **I**) and non-*d*H (bottom in **L**) patterns. Green dashed lines guide the separation of rhythmic pulses and the remaining oscillations. The region between two red vertical lines indicates the PS region.

Figure 7 Distinguishing between the harmonic structures due to PAC and nonlinear effects. (A) Illustration of *d*H pattern and non-*d*H pattern in the FA-H pattern (top) and corresponding power and bicoherence (middle), AAC (bottom). **(B)** Illustration of *d*H pattern and non-*d*H pattern in the PS-H pattern (top) and corresponding power and bicoherence (middle), AAC (bottom). **(C)** The region of interest (ROI) is divided according to the first three frequency bands in the bicoherence plane. The diagonal represents a symmetry axis: ROIs in the lower part of the plane are the same as ROIs in the upper part of the plane. ROI1=

[f_{1st}; f_{1st}]; ROI2= [f_{1st}; f_{2st}]; ROI3= [f_{1st}; f_{3st}]; ROI4= [f_{2st}; f_{2st}]; ROI5= [f_{2st}; f_{3st}]; ROI6= [f_{3st}; f_{3st}]; f_{1st}: the first frequency band, f_{2st}: the second frequency band, f_{3st}: the third frequency band. **(D)** The maximal bicoherence comparison between the *d*H pattern zone and the non-*d*H pattern zone. All ROIs demonstrated higher bicoherence in the *d*H pattern compared to those in the non-*d*H pattern. TFM: time frequency map; AAC: amplitude-amplitude coupling.

Figure 1

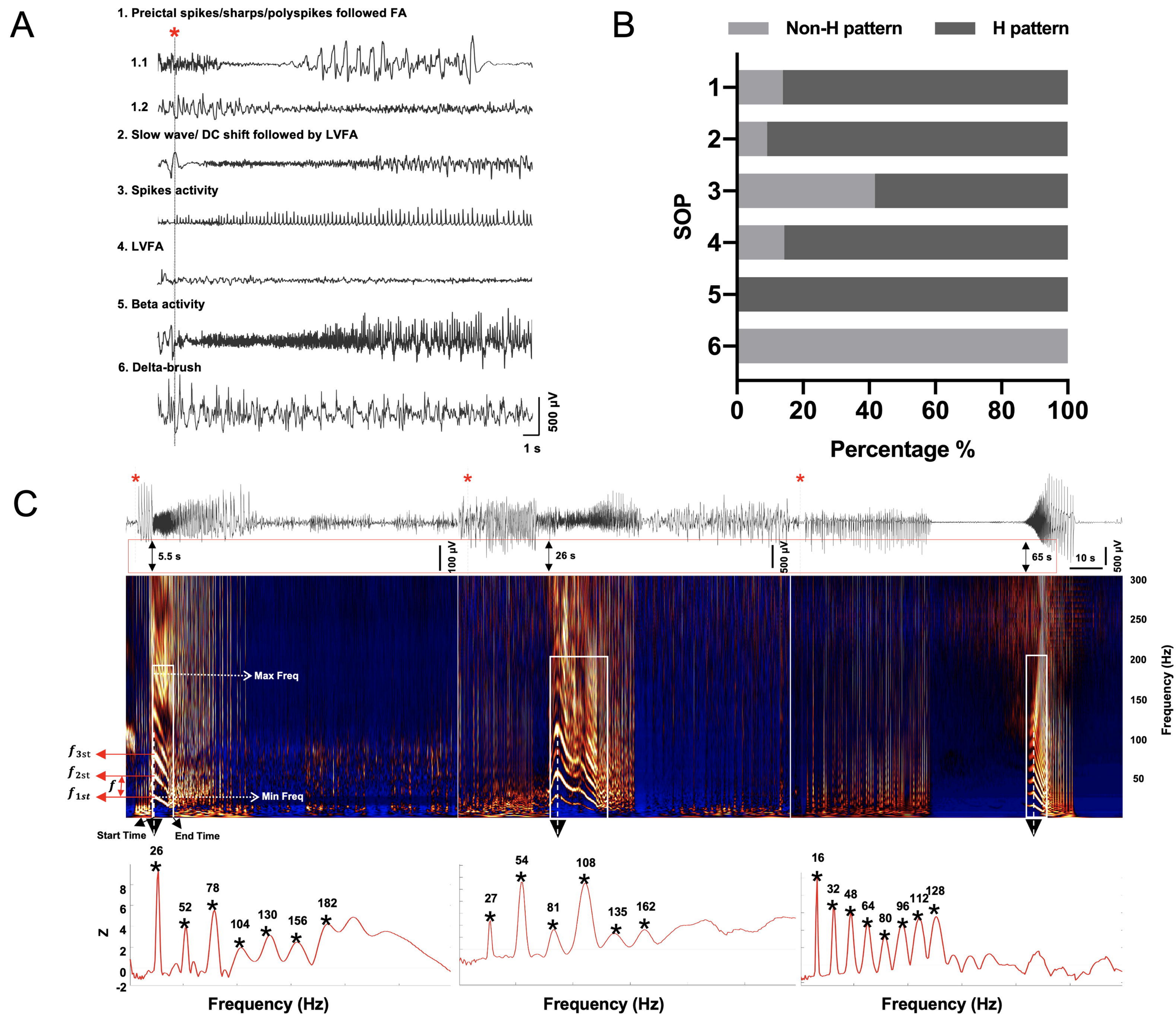
A
1. Preictal spikes/sharps/polyspikes followed FA
1.1
1.2
2. Slow wave/ DC shift followed by LVFA
3. Spikes activity
4. LVFA
5. Beta activity
6. Delta-brush
500 µV
1 s
B
Non-H pattern
H pattern
SOP
1
2
3
4
5
6
0
20
40
60
80
100
Percentage %
C
5.5 s
100 µV
26 s
500 µV
65 s
10 s
500 µV
Max Freq
Min Freq
f_{3st}
f_{2st}
f
f_{1st}
Start Time
End Time
Frequency (Hz)
300
250
200
150
100
50
Z
8
6
4
2
0
-2
26
52
78
104
130
156
182
27
54
81
108
135
162
16
32
48
64
80
96
112
128
Frequency (Hz)
Frequency (Hz)
Frequency (Hz)

Figure 2

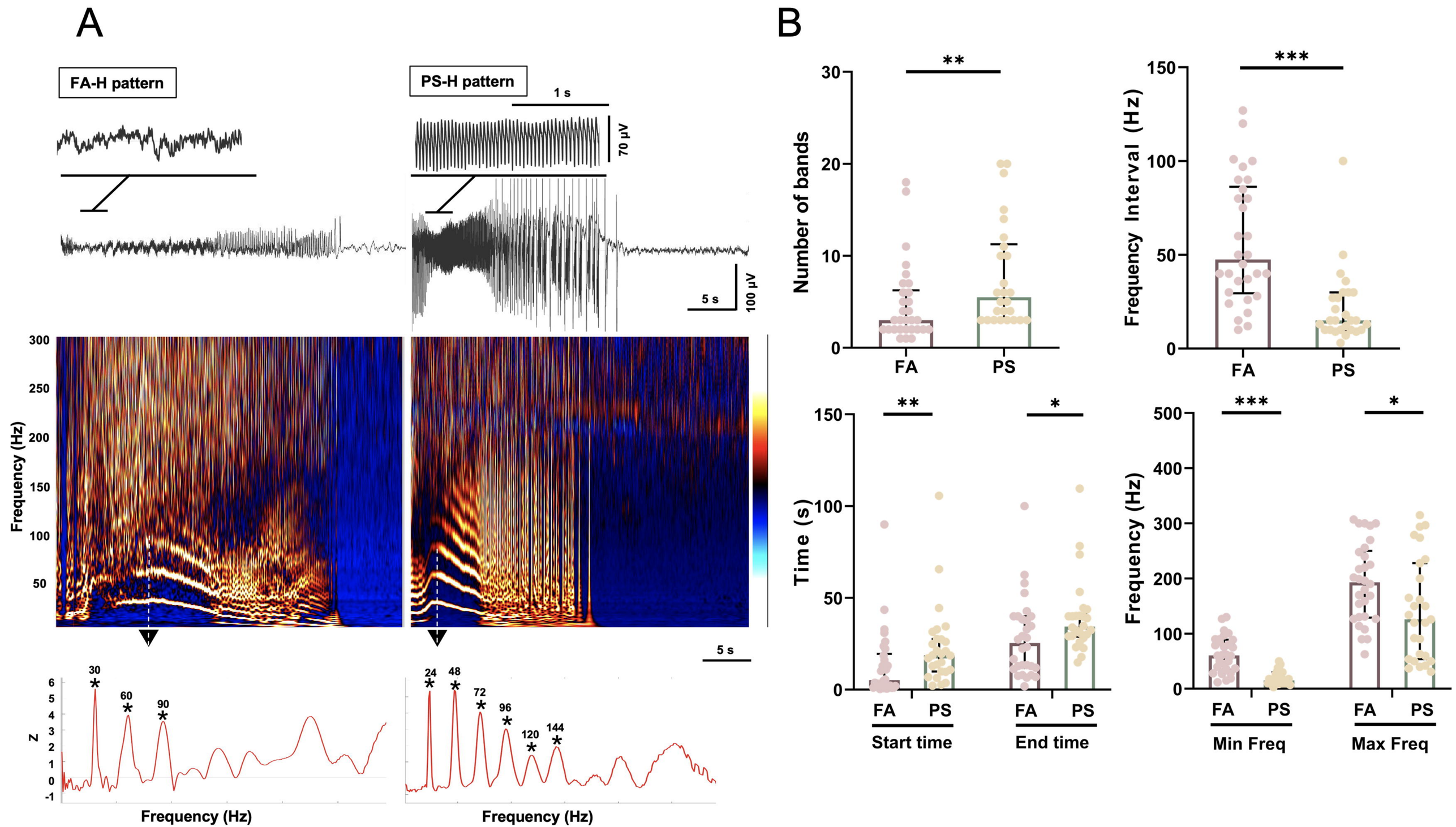
A
FA-H pattern
PS-H pattern
1 s
70 µV
5 s
100 µV
Frequency (Hz)
300
250
200
150
100
50
5 s
30
60
90
24
48
72
96
120
144
Z
Frequency (Hz)
Frequency (Hz)
B
Number of bands
Frequency Interval (Hz)
Time (s)
Frequency (Hz)
FA
PS
Start time
End time
Min Freq
Max Freq
**
***
*

Figure 3

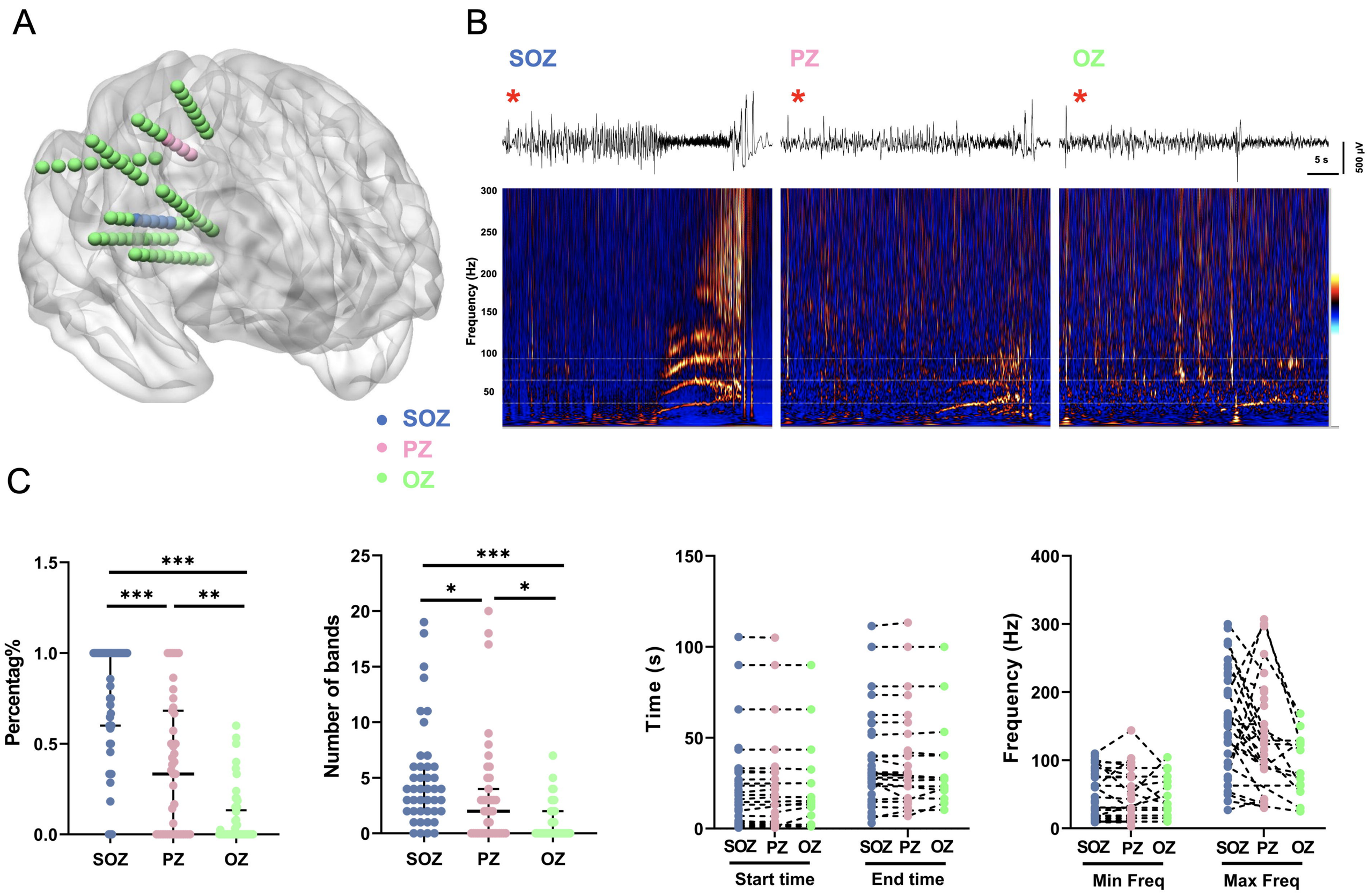
A
SOZ
PZ
OZ
B
SOZ
PZ
OZ
5 s
500 µV
Frequency (Hz)
300
250
200
150
100
50
C
Percentag%
1.5
1.0
0.5
0.0
***
***
**
SOZ
PZ
OZ
Number of bands
25
20
15
10
5
0
***
*
*
Time (s)
150
100
50
0
SOZ PZ OZ
Start time
End time
Frequency (Hz)
400
300
200
100
0
Min Freq
Max Freq

Figure 4

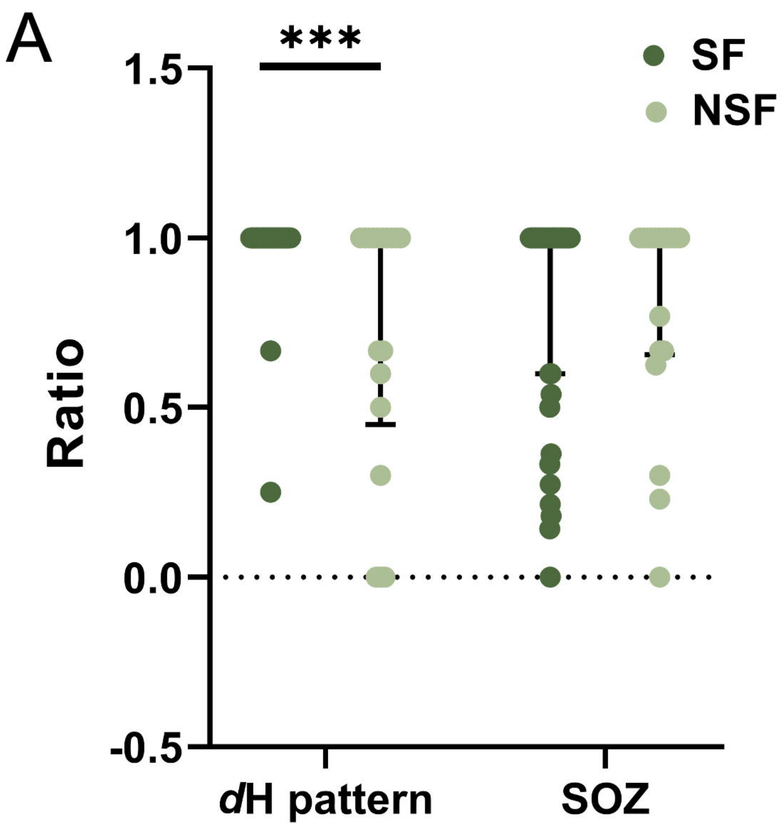
A
***
SF
NSF
1.5
1.0
0.5
0.0
-0.5
Ratio
dH pattern
SOZ

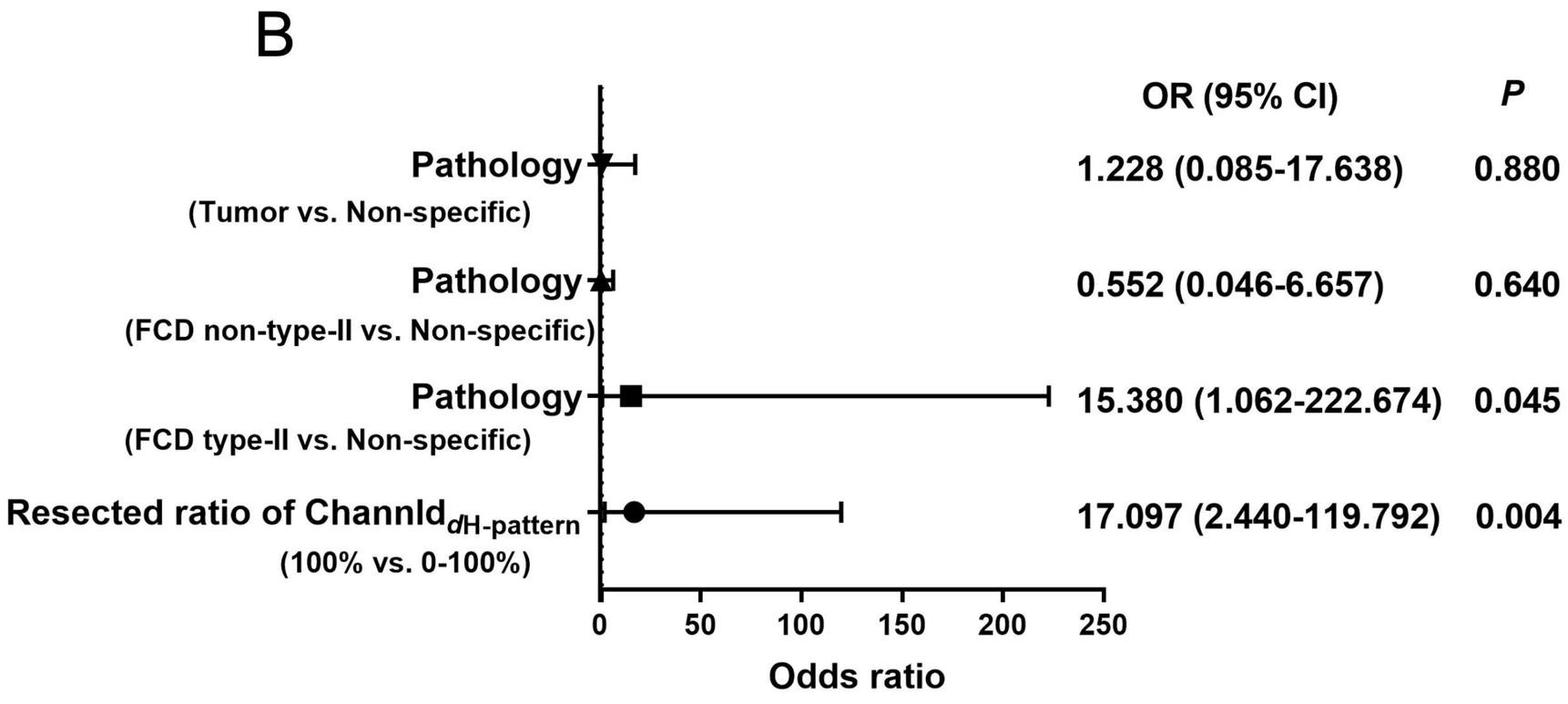
B
OR (95% CI)
P
Pathology
(Tumor vs. Non-specific)
1.228 (0.085-17.638)
0.880
Pathology
(FCD non-type-II vs. Non-specific)
0.552 (0.046-6.657)
0.640
Pathology
(FCD type-II vs. Non-specific)
15.380 (1.062-222.674)
0.045
Resected ratio of ChannId dH-pattern
(100% vs. 0-100%)
17.097 (2.440-119.792)
0.004
0
50
100
150
200
250
Odds ratio

Figure 5

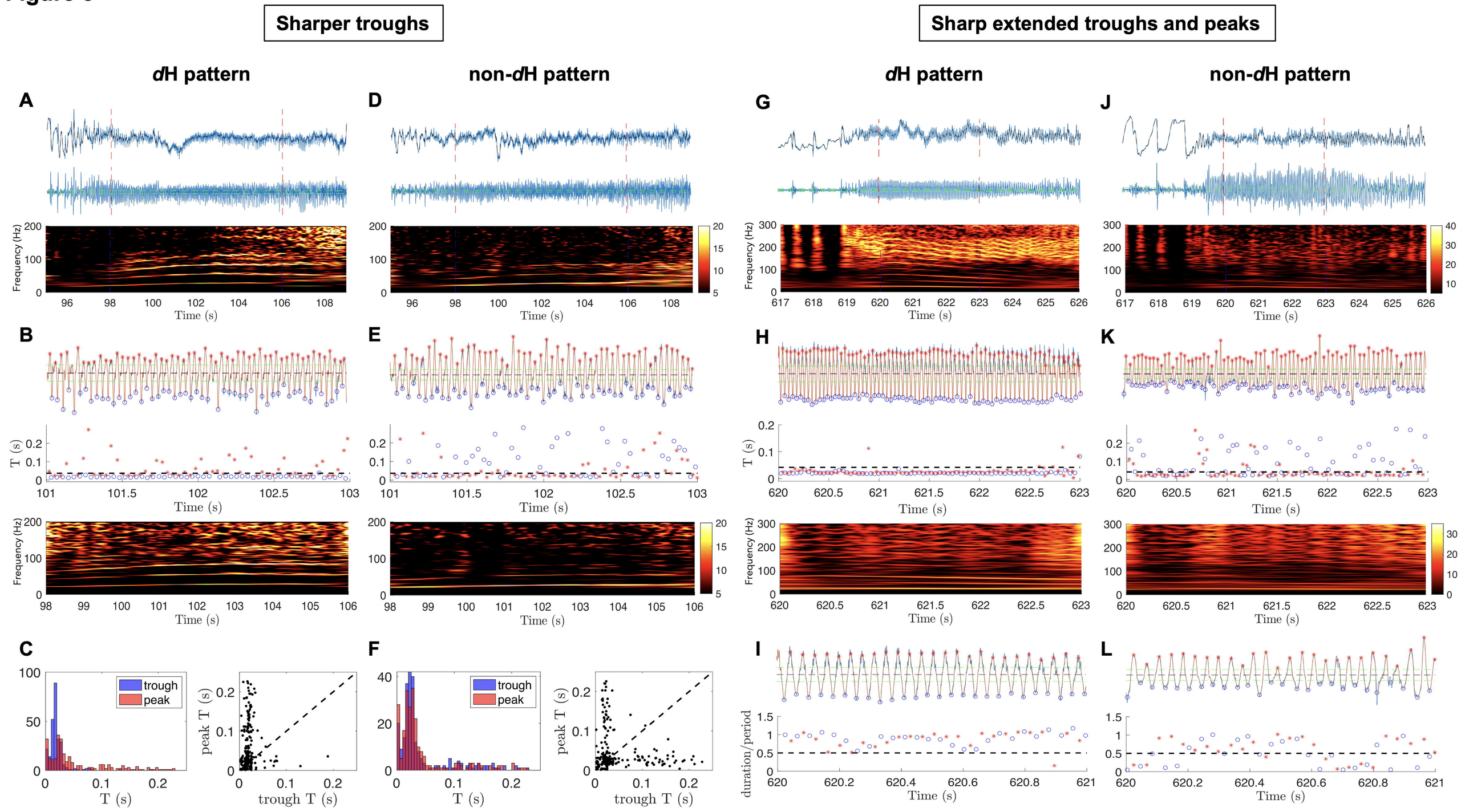
Sharper troughs
Sharp extended troughs and peaks
dH pattern
non-dH pattern
dH pattern
non-dH pattern
A
B
C
D
E
F
G
H
I
J
K
L
Frequency (Hz)
Time (s)
T (s)
peak T (s)
trough T (s)
duration/period
trough
peak

Figure 6

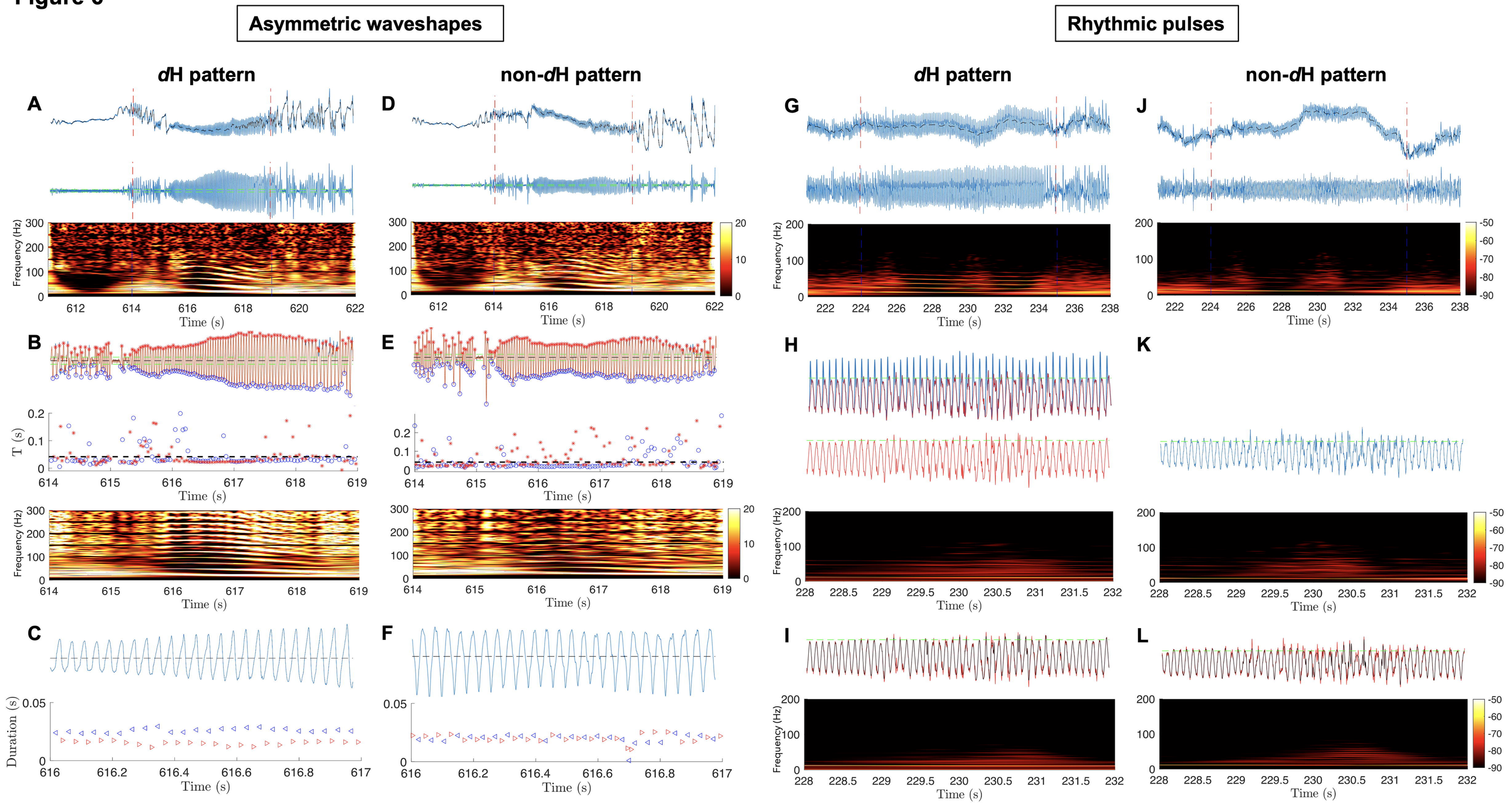
Asymmetric waveshapes
Rhythmic pulses
dH pattern
non-dH pattern
dH pattern
non-dH pattern
A
B
C
D
E
F
G
H
I
J
K
L
Frequency (Hz)
T (s)
Duration (s)
Time (s)

Figure 7

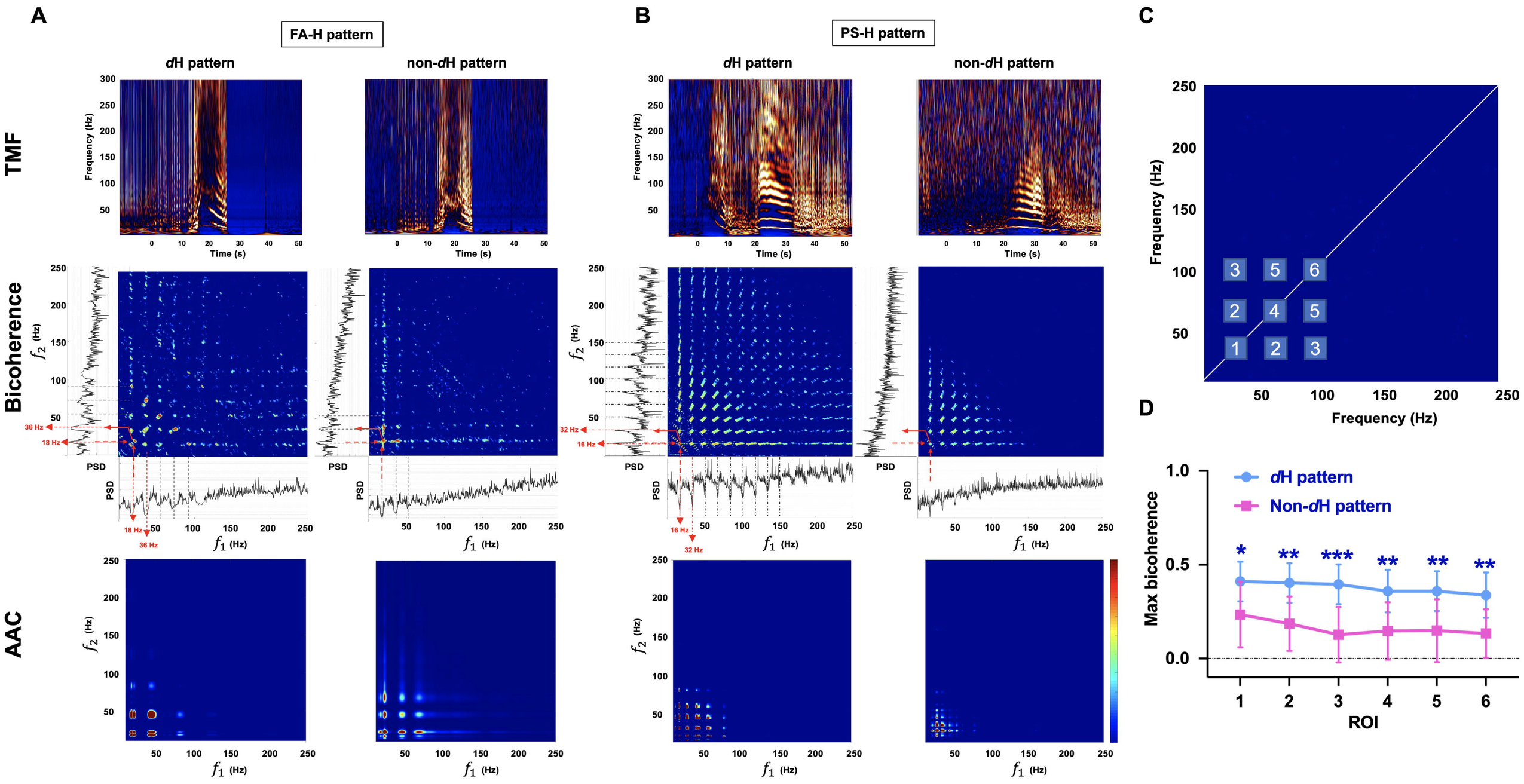
A
FA-H pattern
dH pattern
non-dH pattern
TMF
Frequency (Hz)
Time (s)
Bicoherence
f_2 (Hz)
f_1 (Hz)
PSD
36 Hz
18 Hz
AAC
B
PS-H pattern
32 Hz
16 Hz
C
D
dH pattern
Non-dH pattern
Max bicoherence
ROI
*
**
***

Table 1 Clinical characteristics and surgical outcomes in patients with focal onset pattern on SEEG

	Total (n = 57)	Seizure-free (Engel class Ia) (n = 39)	Not-seizure free (> Engel class Ia) (n = 18)	*P* value
Gender, M, n (%)	31 (54.4 %)	20 (51.3 %)	11 (61.1 %)	0.574[a]
Age at onset, y	10.4±8.5	9.4±7.5	12.6±10.2	0.193[a]
Age at surgery, y	23.6±12.3	23.6±12.8	23.7±11.3	0.991[a]
Epilepsy duration, y	13.3±11.2	14.2±11.8	11.1±9.6	0.329[a]
EEG segments with H pattern, FA/PS	30/27	20/19	10/8	0.784[b]
Lateralization, L, n (%)	26 (45.6 %)	18 (46.2 %)	8(44.4 %)	1.000[b]
Contact number	94.7±29.1	86.5±22.9	112.5±33.4	0.262[a]
Epileptogenic lesion on MRI, n (%)	49 (85.9 %)	35 (89.7 %)	14 (77.8 %)	0.414[c]
Localization, n (%)				0.243[c]
Temporal	20 (35.1 %)	10 (25.6 %)	10 (55.6 %)	
Frontal	24 (42.1 %)	18 (46.2 %)	6(33.3 %)	
Parietal	4(7.0 %)	3 (7.7 %)	1(5.6 %)	
Occipital	4(7.0 %)	4(10.3 %)	0(0.0 %)	
Multi-lobar	5(8.8 %)	4(10.3 %)	1(5.6 %)	
Pathology, n (%)				0.004[c]
Hippocampal sclerosis	6(10.5 %)	5 (12.8 %)	1 (5.6 %)	
Focal cortical dysplasia type II	28 (49.1 %)	23 (59 %)	5 (27.8 %)	
Focal cortical dysplasia (non-type II)	11 (19.3 %)	7(17.9 %) [d]	4 (22.2 %) [d]	
Tumor	2 (3.5 %)	2(5.1 %)	0(0.0 %)	
gliosis/non-specific	10 (17.5%)	2 (5.1 %) [e]	8 (44.4 %) [e]	

Abbreviations: SEEG: Stereo-electroencephalography. M: male; y: years; H pattern: harmonic pattern; FA: fast activity; PS: periodic spike; L: left; MRI: magnetic resonance imaging; SF: seizure free; NSF: not seizure free. Data are presented as the number of patients for categorized variables and the mean ± standard deviation for continuous variables. a. Unpaired t-test. b. Pearson's chi-square test. c. Fisher exact test. d & e. Bonferroni correction: In the SF and NSF groups, there was a discrepancy in pathological finding (p = 0.004). A significant difference was found between FCD II and gliosis/non-specific findings.